The Insulated Solar *Fenton* Hybrid Process: Fundamental Investigations

by **Gerd Sagawe**, **Alexander Lehnard**, **Michael Lübber**, and **Detlef Bahnemann***

Institut für Solarenergieforschung GmbH Hameln/Emmerthal, Aussenstelle Hannover, Sokelantstrasse 5, D-30165 Hannover

Dedicated to Professor *André M. Braun* on the occasion of his 60th birthday

With the so-called advanced oxidation processes (AOPs) gaining more and more importance, the *Fenton* process has proven to be a particularly effective method for the treatment of wastewater. 4-Nitrophenol (4-NP) was selected as the model pollutant to study the influence of temperature and solar illumination on its degradation rate in batch *Fenton* and photo-*Fenton* experiments. Based upon these results, the insulated solar *Fenton* hybrid (ISFH) process was developed, combining solar-chemical and solar-thermal processes. With a flat-plate reactor, it was found to be of particular importance to determine the optimal reactor depth for this continuous process, since excessive reactor depth increased the heat capacity, resulting in an increase of the heating period. Constructive limits were also clearly established.

Introduction. – The so-called advanced oxidation processes (AOPs)[1]) have gained increasing importance for the treatment of polluted water in recent years. It is the common feature of all these processes that highly reactive hydroxyl radicals are generated, a species that is able to mineralize almost all toxic and biologically nondegradable compounds present in the water matrix [1]. Unlike classical treatment methods such as adsorption or air stripping, AOPs avoid typical phase-transfer problems.

The *Fenton*, and also the photo-*Fenton* process, play key roles among these AOPs with the hydroxyl radicals being formed from hydrogen peroxide with Fe^{II}/Fe^{III} as a catalytic couple. The rate of the overall detoxification process involving these iron salts can be considerably increased *via* photochemical reactions induced by irradiation with light between 200 and 500 nm [2–6], and it was shown that the sun can be a very useful light source for this purpose in the wavelength range above 300 nm [2–4][7][8]. Several pilot plants for the practical application of the photo-*Fenton* process have been tested (see, *e.g.*, [2][9–12]).

In general, the rate of the pollutant degradation increases with increasing temperature. When wastewater contains high concentrations of organic compounds, the exothermic *Fenton* and photo-*Fenton* processes can deliver enough energy to heat the wastewater, yielding higher reaction rates at elevated temperatures [13]. In the case of moderate or low concentrations of organic substances, other energy sources have to be used to heat the wastewater if the process should operate at elevated temperatures. Thus, a combination of photochemical and thermal utilization of solar energy should result in optimal reaction conditions. While the photochemical utilization of solar irradiation for this process is feasible only at wavelengths below 500 nm [2–4][7][8],

[1]) See *Glossary* (below).

solar-thermal energy from the entire spectrum of the sun is useful. We have, therefore, developed the so-called insulated solar *Fenton* hybrid (ISFH)[1]) process, which employs a suitable insulation of the photoreactor and a heat exchanger to transfer thermal energy from the treated water stream to the incoming water flow. Thus, operating temperatures well above the ambient temperature could be realized for the solar photo-*Fenton* process [14].

Herein we report the results of basic batch experiments employing 4-nitrophenol (4-NP)[1]) as a suitable model pollutant studying the influence of parameters such as temperature and reactor depth on its degradation rate in both, the *Fenton* as well as the photo-*Fenton* process. The results of this study were important for planning and constructing a first pilot plant for the ISFH process, which in the meantime has been realized.

Basic Principles. *Chemical Basics of the* Fenton *and the Photo*-Fenton *Processes.* – Very reactive hydroxyl radicals $OH^{\cdot}$ are formed when ferrous (Fe^{II}) salts react with hydrogen peroxide. While *Fenton* discovered this reaction as early as 1894 [15], it took a long time for researchers to realize that these $OH^{\cdot}$ radicals can conveniently be utilized to oxidize and finally mineralize organic contaminants present in the water matrix [8]. *Eqn. 1* summarizes the net reaction occurring in the *Fenton* process. Details of the underlying reaction mechanism have been studied extensively [3][4][6][16]. It is the initial *Fenton* reaction (*Eqn. 2*) that yields the reactive $OH^{\cdot}$ radicals. In the presence of organic compounds (RH), these $OH^{\cdot}$ radicals are known to react in almost diffusion-controlled reactions *via* H-abstraction (*Eqn. 3*) or electrophilic addition (*Eqn. 4*).

$$RX + xH_2O_2 \xrightarrow{Fe^{3+}/Fe^{2+},\ pH3} yCO_2 + zH_2O + \text{mineral salts} \quad (1)$$

$$Fe^{2+} + H_2O_2 \rightarrow Fe^{3+} + OH^- + OH^{\cdot} \quad (2)$$

$$OH^{\cdot} + RH \rightarrow H_2O + R^{\cdot} \quad (3)$$

$$OH^{\cdot} + \diagdown\!\!>C{=}C<\!\!\diagup \rightarrow HO-\overset{|}{\underset{|}{C}}-\overset{|}{\underset{|}{C}}{}^{\cdot} \quad (4)$$

Ferric ions Fe^{3+} formed in *Eqn. 2* are subsequently reduced back to Fe^{2+} (*Eqns. 5–7*) which is needed for the continuation of the *Fenton* reaction. Thus, the different iron salts clearly act as catalysts in the overall process. Additionally, radical recombination reactions like that of *Eqn. 8* have to be considered.

$$Fe^{3+} + H_2O_2 \rightarrow Fe^{2+} + HO_2^{\cdot} + H^+ \quad (5)$$

$$Fe^{3+} + R^{\cdot} \rightarrow Fe^{2+} + R^+ \quad (6)$$

$$Fe^{3+} + HO_2^{\cdot} \rightarrow Fe^{2+} + O_2 + H^+ \quad (7)$$

$$HO_2^{\cdot} + HO_2^{\cdot} \rightarrow H_2O_2 + O_2 \quad (8)$$

In principle, the reactions of *Eqns. 2* and *5–7* establish a chain reaction leading to the continuous formation of $OH^{\cdot}$ radicals and, therefore, to the continuous degradation of

the organic contaminants *via Eqns. 3* and *4*. Consequently, H_2O_2 for the *Fenton* process can be used in large excess compared with the initial concentration of the iron salt. However, due to the usually very small steady-state concentration of the free radical species $R^{\cdot}$ and $HO_2^{\cdot}$ or the small rate constant of the reaction of *Eqn. 5*, the regeneration of Fe^{2+} is rate-limiting for the overall process. It should be noted that, in spite of these limitations, the overall process can also be started according to the reaction sequence of *Eqns. 5* and *2* from Fe^{3+} ions.

The organic radicals formed in *Eqns. 3* and *4* will subsequently be mineralized in the presence of dissolved molecular O_2 (*Eqn. 9*), which is formed continuously in the system through reactions such as *Eqn. 7*, or alternative reactions not shown here, but can also be supplied, *e.g.* by purging with air. Moreover, peroxide dismutation (*Eqn. 10*) also yields O_2 resulting in the undesired consumption of hydrogen peroxide.

$$R^{\cdot} + O_2 \xrightarrow[Fenton]{OH^{\bullet}} \xrightarrow{\Delta} CO_2 + H_2O + \ldots. \tag{9}$$

$$2\,H_2O_2 \rightarrow 2\,H_2O + O_2 \tag{10}$$

The reactions of *Eqns. 11–13* represent other important side reactions of the *Fenton* process, which are also highly undesirable.

$$OH^{\cdot} + H_2O_2 \rightarrow H_2O + HO_2^{\cdot} \tag{11}$$

$$OH^{\cdot} + Fe^{2+} \rightarrow Fe^{3+} + OH^{-} \tag{12}$$

$$R^{\cdot} + Fe^{2+} \rightarrow R^{-} + Fe^{3+} \tag{13}$$

The involvement of many additional free-radical reactions in the *Fenton* process has been discussed extensively in the literature [2–4][8][10][17–19]. Moreover, Fe^{4+} has been proposed as the main reactive intermediate besides $OH^{\cdot}$ [17][18]. The highest overall reaction rates for the *Fenton* process are found at *ca.* pH 3. At higher pH values, ferric ions are likely to form insoluble hydroxide complexes.

The photo-*Fenton* process executes the *Fenton* process (*Eqns. 1–13*) in the presence of irradiation with light between 200 and 500 nm [2][4]. The main light-absorbing species in the *Fenton* system are ferric ion complexes, *i.e.* $[Fe(OH)]^{2+}$ and $[Fe(RCO_2)]^{2+}$, which will yield additional Fe^{2+} following photoinduced ligand-to-metal charge-transfer (LMCT)[1]) reactions (*Eqns. 14* and *15*).

$$[Fe^{3+}(OH)^{-}]^{2+} \xrightarrow{h\nu} Fe^{2+} + OH^{\cdot}\ (\lambda < ca.\ 450\ \text{nm}) \tag{14}$$

$$[Fe^{3+}(RCO_2)^{-}]^{2+} \xrightarrow{h\nu} Fe^{2+} + CO_2 + R^{\cdot}\ (\lambda < ca.\ 500\ \text{nm}) \tag{15}$$

Additionally, *Eqn. 14* yields $OH^{\cdot}$ radicals, while *Eqn. 15* results in a reduction of the total organic carbon (TOC)[1]) content of the system due to the decarboxylation of organic-acid intermediates. Since both LMCT reactions will form the ferrous ions required for the *Fenton* reaction (*Eqn. 2*), the overall degradation rate of organic compounds is considerably increased in the photo-*Fenton* process, even at lower

concentrations of iron salts present in the system [3]. Complexing organic acids (RCO_2^-) can either be added to the wastewater in form of, *e.g.*, oxalic acid [4] [17], or will be formed during the degradation of organic pollutants.

The ISFH (Insulated Solar Fenton *Hybrid) Process.* Since the reaction rate of the rate-limiting steps of the *Fenton* process, *e.g. Eqns. 5 – 7*, can be considerably enhanced at elevated temperatures, and since light between 200 and 500 nm increases the rate of the overall process through *Eqns. 14* and *15*, it is an obvious approach to combine thermal and photochemical enhancement to reach optimized reaction conditions. The use of solar photons appears to be particularly attractive for this purpose as the solar spectrum contains UV/VIS photons required for the photochemical processes as well as IR photons delivering sufficient thermal energy to carry out the process at low solute concentrations and/or low levels of iron salts and hydrogen peroxide. Consequently, we have developed the ISFH process, which combines a thermally insulated photoreactor and a heat exchanger that transfers heat from the effluent water stream to preheat the influent water before entering the photoreactor [14]. The optimal building material for the photoreactor should, therefore, be transparent for all the wavelengths of the solar spectrum. *Fig. 1* shows a possible setup for a continuously operated ISFH process. The process scheme includes the optional flocculation and sedimentation of the ferric hydroxide sludge. The sludge can be recycled after dissolution by different methods, or it can be deposited. The flat-plate photoreactor, *e.g.*, can consist of a double-skin sheet reactor (DSSR)[1]) made from UV-A-transparent poly(methyl acrylate) (PMMA)[1]), which previously has been tested successfully for the photocatalytic water treatment [20][21]. At the front side of the DSSR, a UV-A-transparent acrylic glass cover can prevent heat loss while enabling the transmission of photons over the whole solar spectrum. The back side of the DSSR can be painted black to absorb the transmitted solar radiation and to transform it into thermal energy to be used to heat the

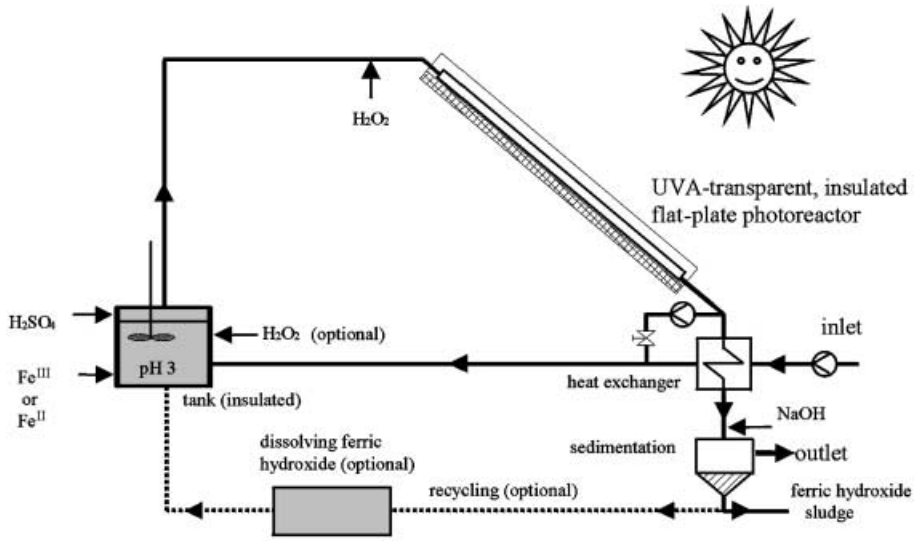

Fig. 1. *Typical schematic process scheme of the ISFH process*

wastewater inside the DSSR. Except for the front side, the photoreactor can be insulated to minimize thermal-heat losses.

However, besides flat-plate reactors, also slightly light-concentrating reactors such as compound parabolic collectors (CPCs)[1]) or strongly concentrating parabolic trough reactors (PTRs)[1]) can conveniently be employed for the ISFH process.

Due to the interdependence of the absorption of light, the photochemical effects, the process temperature, and the temperature-dependant reaction rates, the ISFH process presents an interesting engineering challenge with the importance to simulate the so-called inner-filter effect during the process. Thereby, it is important to consider that the rate of degradation, especially in the case of the photo-*Fenton* process, is affected by the reactor geometry [11][22].

Materials and Methods. *Experimental Setup.* Experiments for the *Fenton* process were carried out in a thermostated, well-stirred 500-ml *Erlenmeier* flask, which was well-shielded against incoming light. The experimental setup to study the photo-*Fenton* reactions is shown in *Fig. 2*. It mainly consists of an open rectangular batch photoreactor with an illuminated area $A_{inc} = 0.077\ m^2$. To minimize the influence of the reactor walls on the light field within the photoreactor, the side walls of the reactor were made from UV-A-transparent poly(methyl methacrylate) (PMMA) and shielded with aluminium foil on the outside. This construction detail prevents outside light from entering the reactor from the sides and reflects photons from within the reactor back in. Thus, the reaction volume will be limited to the reactor volume, while the light field inside the reactor will be identical to that within a photoreactor with infinite dimensions in the plane of irradiation. This enabled the simulation of the conditions in a large flat-plate reactor by means of a small one on the laboratory scale. The total liquid volume inside the photoreactor, and hence also the reactor depth, could be adjusted by changing the filling height inside the reactor. Thereby, the filling height represents the distance between the reactor bottom and the illuminated surface of the solution, which also will be defined as the reactor depth. As in the case of the *Fenton* reactor, the solution inside the photo-*Fenton* reactor setup was well-stirred and thermostated.

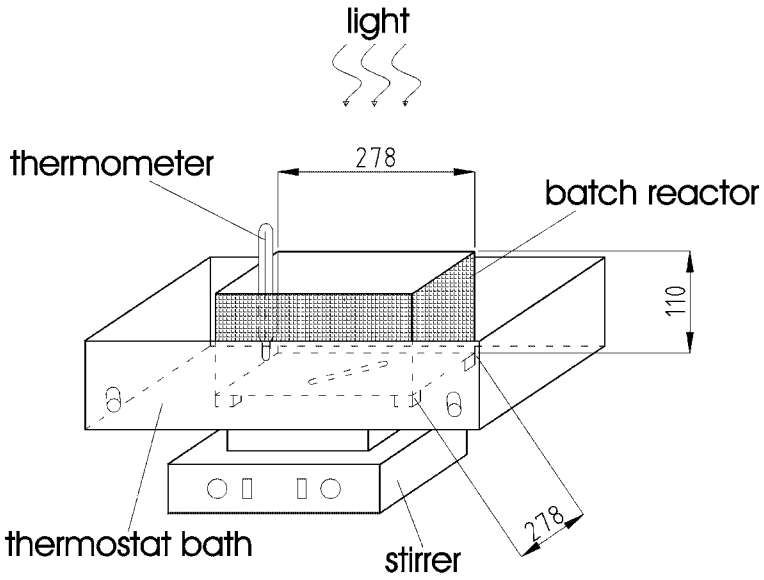

Fig. 2. *Unsteady batch reactor in thermostat bath* (distances in mm)

An artificial solar irradiation field was constructed for all photo-*Fenton* experiments (*Fig. 3*). It was produced by two solar simulation lamps *SOL 1200* (*Dr. Hönle UV Technik*) which, as shown in *Fig. 4* (see below), possess an emission spectrum very similar to the AM-1.5[1]) spectrum of the sun at the earth's surface. A very homogeneous light field with a mean UV-A irradiance of $q_{UV} = 57.5 \pm 2.5\ W \cdot m^{-2}$ [1]) at the surface of the reactor was achieved through the integration of reflectors made from aluminium at all sides of the illumination unit (see *Fig. 3*). This value is very similar to the maximum measured near the surface of the earth.

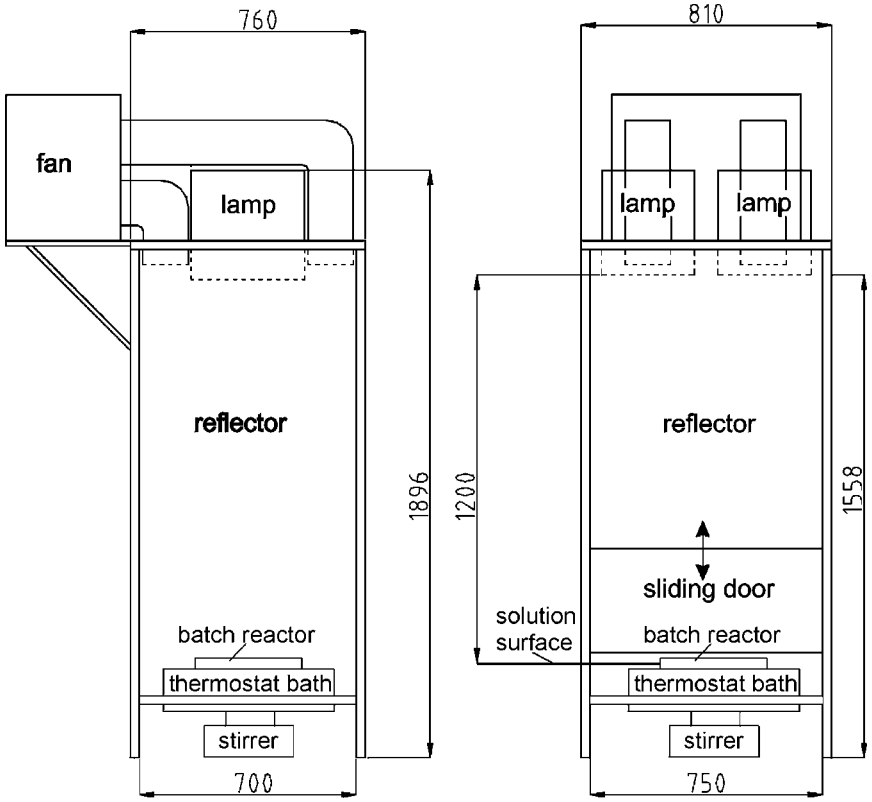

Fig. 3. *Artifical solar irradiation field.* $q_{UV} = 57.5 \pm 2.5\ W \cdot m^{-2}$ (distances in mm)

Chemicals and Analytical Methods. All chemicals used throughout this study were of the highest commercially available grade and used without further purification. The water used was *Millipore-RO* treated (resistivity > 18 MΩ · cm). 4-NP was employed as the model pollutant for all degradation experiments with the initial concentration $c_0(\text{4-NP}) = 0.5\ \text{mmol} \cdot \text{l}^{-1}$. Dil. H_2SO_4 soln. was used to acidify the soln. before adding $Fe_2(SO_4)_3 \cdot H_2O$ ($c_0(Fe^{3+}) = 0.05\ \text{mmol} \cdot \text{l}^{-1}$). NaOH was used to adjust the pH value to pH 3. The experiments were started by adding H_2O_2 ($c_0(H_2O_2) = 5.0\ \text{mmol} \cdot \text{l}^{-1}$) and, in the case of the photo-*Fenton* system, by simultaneously beginning with the illumination.

The concentration of 4-NP was measured in aliquots taken at regular intervals during the reaction by HPLC (*Dionex* series *4500i* chromatograph, *Dionex* variable-wavelength detector at λ 270 nm, column *Nucleosil 100-10-C18*). Prior to these measurements, all samples were stabilized with sodium acetate as the pH buffer and radical scavenger and with catalase (*Micrococcus Iyodeikticus*, 10 µl) to destroy hydrogen peroxide. This treatment was used to stop the reaction within the samples immediately upon removal from the reactor.

A *Shimadzu* TOC analyser *TOC 5000* was used to measure the total organic carbon (TOC)[1]) content of the samples. UV/VIS Spectra: *Perkin-Elmer Lambda-17* UV/VIS spectrophotometer. The irradiance in the UV-A region was measured with a radiometer (*Dr. Hönle UV-Technik*).

Results. – The main purpose of this work was to collect relevant data required to determine the efficiency of the ISFH process and to design the first pilot plant for its realization. Therefore, we investigated the influence of the reaction temperature on the degradation rate of the model compound 4-NP for both the *Fenton* and the photo-*Fenton* processes. Moreover, the influence of the reactor depth on the 4-NP degradation rate was also studied in detail for the photo-*Fenton* process. The model compound 4-NP was chosen for its environmental importance, its aromatic structure, and its strong light absorption up to 400 nm at pH 3. Such a strong absorption of UV-A light is typical for most real wastewater. The degradation rates of photochemical processes depend on the concentrations of all substances, including the degradation products, in the solution, the temperature, and the light distribution inside the photoreactor. The light distribution itself depends on the illumination, the reactor geometry, and the time-dependant inner-filter effect caused by all substances present in solution. Thus, from an engineering point of view, the model pollutant 4-NP combines the advantage of a well-characterized substance to study the photochemical process, with the simulation of the inner-filter effect typical for real wastewater. This is very important for any reactor scale-up, especially if the influence of the reactor geometry on the process itself is to be investigated. Several models to account for light-field distributions inside different kinds of photoreactors are presented in [23].

The UV/VIS absorption spectrum of aqueous solutions of 4-NP, $Fe_2(SO_4)_3$, and H_2O_2, respectively, is shown in *Fig. 4*, together with the spectrum of the model solution as it was employed for the experiments carried out in this work (pH 3, optical pathlength 1.0 cm). Also shown is the AM-1.5 spectrum typical for the solar radiation reaching the surface of the earth [24] and the spectral irradiance at the top of the photoreactor inside the irradiation setup. The spectral irradiance at this surface was calculated by means of the relative lamp spectra $q_{\lambda\mathrm{rel}}$ known from the product information of the lamps [25], measuring the irradiance q_{UV} in the UV-A region with the UV-A detector described above, and employing *Eqns. 16* and *17*[1]). Thereby, the reference irradiance q_{ref} can be obtained from *Eqn. 16*, while the spectral irradiance q_λ is then calculated *via Eqn. 17* after rearrangement. The use of these relations implies that the spectral distribution is not influenced by the irradiation setup itself. Because the photo-*Fenton* process can utilize light up to *ca.* 500 nm, it is of importance to know the irradiance for the wavelength range 300–500 nm. Applying *Eqn. 17* up to 500 nm (see *Eqn. 18*), the irradiance $q_{<500\,\mathrm{nm}}$ can be calculated in energetic or stoichiometric units to be $q_{<500\,\mathrm{nm}} = 176\ \mathrm{W\cdot m^{-2}}$ or $q_{<500\,\mathrm{nm}} = 6.13\cdot 10^{-4}\ \mathrm{Einstein\cdot m^{-2}\cdot s^{-1}}$.

$$q_{\mathrm{UV}} = \int_{300\,\mathrm{mm}}^{400\,\mathrm{mm}} q_\lambda \mathrm{d}\lambda = q_{\mathrm{ref}} \int_{300\,\mathrm{mm}}^{400\,\mathrm{mm}} q_{\lambda,\mathrm{rel}} \mathrm{d}\lambda \tag{16}$$

$$q_{\lambda,\mathrm{rel}} = \frac{q_\lambda}{q_{\mathrm{ref}}} \tag{17}$$

$$q_{<500\mathrm{nm}} = \int_{300\,\mathrm{nm}}^{500\,\mathrm{nm}} q_\lambda \mathrm{d}\lambda \tag{18}$$

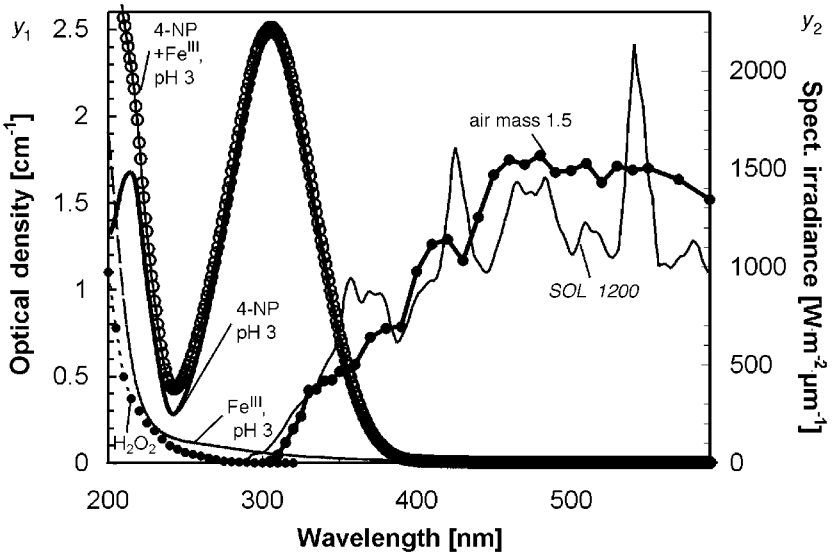

Fig. 4. *Absorption spectra of aqueous solutions containing 4-NP, $Fe_2(SO_4)_3$, or hydrogen peroxide, and of the model solution at concentrations used in the experiments* (c(4-NP) = 0.5 mmol·l^{-1}, $c(H_2O_2)$ = 5.0 mmol·l^{-1}, $c(Fe^{3+})$ = 0.05 mmol·l^{-1}, pH 3.0) (Y_1 axis, optical density). *Solar spectrum at air mass* (AM) *1.5 and the spectrum of the lamps (SOL 1200) used for the irradiation setup* (Y_2 axis, spectral irradiance).

While the absorption spectrum of the aqueous ferric solution extends into the VIS region of the solar spectrum, *i.e.*, up to 450 nm, the solution containing only hydrogen peroxide does not exhibit any absorption beyond 270 nm, evincing that solar photons will not be able to induce the splitting of H_2O_2 into OH· radicals. The absorption of the aqueous 4-NP solution between 270 and 400 nm by far exceeds that of $Fe_2(SO_4)_3$ under the chosen experimental conditions. Consequently, the majority of the incoming photons in this spectral region will be absorbed by 4-NP molecules and can thus not be used for the photochemical regeneration of Fe^{3+} (*Eqns. 14* and *15*). These conditions were chosen deliberately since this so-called inner-filter effect is typical for many real wastewaters and has to be taken into account for all photochemical treatment processes. Blank experiments carried out under identical conditions in the absence of H_2O_2 and/or Fe^{3+} showed that the rate of the photolysis of 4-NP can be neglected under the reaction conditions employed.

The absorption spectrum of the model solution agrees very well with the sum of the spectra of its components, evincing that the formation of optically absorbing complexes does not play any significant role in this system initially. Since the magnitude of the optical absorption of the model solution exceeds unity over almost the entire UV region below 400 nm, it is readily calculated that only a minor part of the incident UV light will be able to reach a depth beyond 1.0 cm in the reactor system. The main reaction area for photochemical processes involving a LMCT reaction will, therefore, be the first cm beneath the irradiated water surface. Ferric complexes involving carboxylates RCO_2^-, which are likely to be formed during the course of the reaction, will be able to absorb also VIS light up to 500 nm, thus allowing photochemical

processes in deeper regions of the reactor. However, it should be noted that the model solution employed in this study develops an intensely brown coloration during the course of the reaction that prevents photolytic reactions in greater depths of the reactor.

Typical results obtained during the batch experiments are shown in *Fig. 5* for the 4-NP degradation with the *Fenton* and photo-*Fenton* process, respectively. Also shown is the degradation of the TOC value observed in both systems. While it is obvious that the 4-NP degradation as well as its total mineralization proceeds considerably faster in the photo-*Fenton* process, it is also observed that the mineralization process is, by a factor of *ca*. 3, slower than that of 4-NP depletion in both cases. It is obvious from the results shown in *Fig. 5* that the 4-NP degradation curves consist of three phases. An induction period showing a rather slow degradation of 10% of the initial amount of model compound is followed by an almost linear decay curve up to *ca.* 90% degradation. Finally, the reaction slows down once again until the 4-NP concentration reaches the detection limit. The TOC degradation curve exhibits a similar shape as that of the 4-NP degradation. The following studies were carried out by measurements of the 4-NP concentration, TOC measurements being carried out only at regular intervals for control purposes.

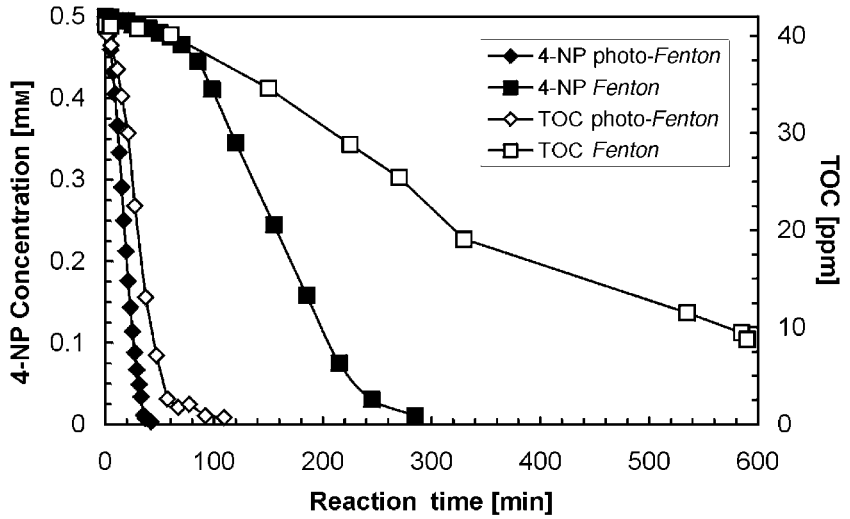

Fig. 5. *4-NP Concentration and TOC as a function of the reaction time.* c_0(4-NP) = 0.5 mmol·l^{-1}, $c_0(H_2O_2)$ = 5.0 mmol·l^{-1}, $c_0(Fe^{3+})$ = 0.05 mmol·l^{-1}, pH 3.0; photo-*Fenton* process: $q_{<500\,nm} = 6.13 \cdot 10^{-4}$ Einstein·m^{-2}·s^{-1}, d = 7.5 cm, ϑ 20°.

Since all kinetics curves exhibit rather complex behavior as described above, we decided to use the so-called reaction rate $r_{90\%}$ to compare degradation experiments carried out under different experimental conditions. $\Delta t_{90\%}$ is the reaction time required to achieve 90% degradation of the model compound. $r_{90\%}$ is than defined by *Eqn. 19*. This average reaction rate $r_{90\%}$ will be used in the following diagrams.

$$r_{90\%} = \frac{\Delta c_{90\%}}{\Delta t_{90\%}} = \frac{0.9 \cdot c_0}{\Delta t_{90\%}} \tag{19}$$

The dependence of the 4-NP degradation rate $r_{90\%}$ on the reaction temperature is shown for the *Fenton* process in *Fig. 6*. It is interesting to note that the rate increases continuously with increasing reaction temperature, the most significant changes being observed above 40°. Thus, while it takes 360 min to degrade 90% of the initially present 4-NP at 20°, only 10 min are required to achieve the same degree of degradation at 70°.

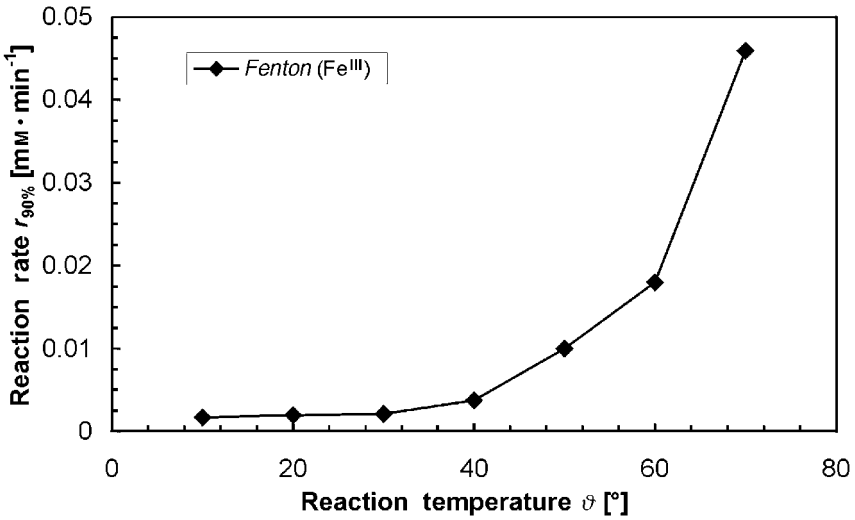

Fig. 6. *Reaction rate* $r_{90\%}$ *of 4NP degradation as a function of the reaction temperature for the* Fenton *process.* c_0(4-NP) = 0.5 mmol · l^{-1}, $c_0(H_2O_2)$ = 5.0 mmol · l^{-1}, $c_0(Fe^{3+})$ = 0.05 mmol · l^{-1}, pH 3.0.

Fig. 7 shows that the reaction temperature also accelerates the 4-NP degradation during the photo-*Fenton* process under simulated solar-illumination conditions. As in the case of the *Fenton* process, the degradation rate steadily increases with increasing reaction temperature, the most significant increase being observed between 30 and 50°. Between 10 and 50°, the time required for 90% degradation of 4-NP($\Delta t_{90\%}$) is reduced by almost exactly 50% with every temperature increase of 10°.

Comparing the results presented in *Figs. 6* and *7* it is apparent that the rate of 4-NP degradation employing the photo-*Fenton* process exceeds that of the *Fenton* process by almost one order of magnitude. At 50°, *e.g.*, it takes less than 2 min to degrade 90% of the initially present 4-NP.

The influence of the reactor depth on the degradation rate of 4-NP was studied at 20 and 50° for the photo-*Fenton* process. The reaction rates $r_{90\%}$ measured at reactor depths between 0.75 and 10 cm are shown in *Figs. 8* and *9* for the reaction temperatures 20 and 50°. In these experiments, the variation of the reactor depth is achieved by changing the volume of the model solution, the reactor depth being the distance between the surface of the illuminated water layer and the reactor bottom. While at 50° $r_{90\%}$ decreases by *ca.* 25% when the reactor depth is increased from 0.75 to 10 cm, it decreases by *ca.* 50% at 20° under otherwise identical conditions.

Discussion. – The importance of UV/VIS irradiation and increased reaction temperature for the 4-NP degradation rate is clearly demonstrated in Fig. 9. While

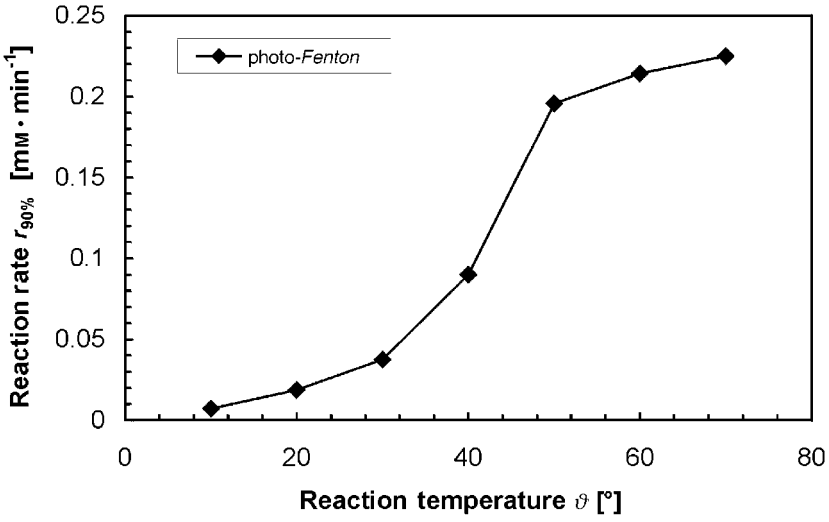

Fig. 7. *Reaction rate* $r_{90\%}$ *of 4-NP degradation as a function of the reaction temperature for the photo*-Fenton *process.* Conditions as in *Fig. 6*, $q_{<500\,nm} = 6.13 \cdot 10^{-4}$ Einstein $\cdot\, m^{-2} \cdot s^{-1}$, reactor depth $d = 5$ cm.

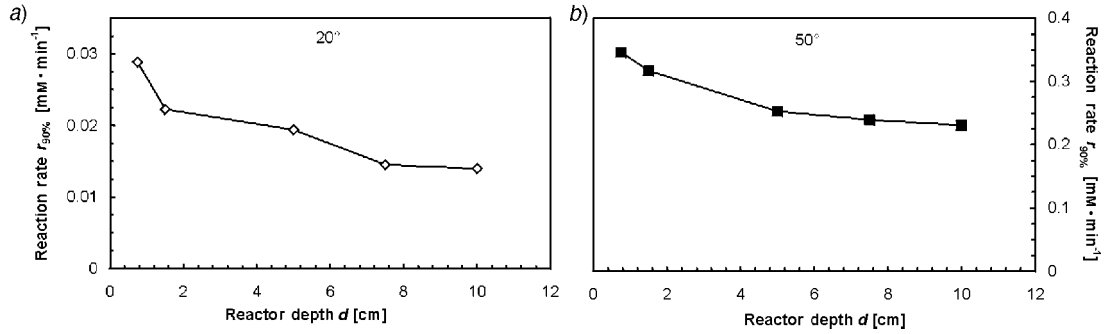

Fig. 8. *Reaction rate* $r_{90\%}$ *of 4-NP degradation as a function of the reactor depth* d *at* a) ϑ 20° and b) ϑ 50°. Conditions as in *Fig. 6*, $q_{<500\,nm} = 6.13 \cdot 10^{-4}$ Einstein $\cdot\, m^{-2} \cdot s^{-1}$.

under the conditions employed in this study, an increase of the reaction temperature from 20 to 50° results in an acceleration of the 4-NP degradation rate by a factor of 5, the photo-*Fenton* reaction can even be accelerated by a factor of 12 under otherwise identical conditions. Comparing the *Fenton* reaction at 20° with the photo-*Fenton* reaction at 50°, a rate increase by more than two orders of magnitude, *i.e.*, by a factor of 125 is observed.

To analyse the temperature dependence in more detail, the data shown in *Figs. 6* and *7* were formally replotted as an *Arrhenius*-type diagram (*Fig. 10*). It is obvious from this presentation that both the *Fenton* as well as the photo-*Fenton* degradations of 4-NP yield reasonably linear dependencies over almost the entire temperature range studied in this $\ln r = f(1/T)$ relationship with almost identical slopes. Apparent *Arrhenius* activation energies $E_a = 49$ and 45 kJ/mol are readily calculated for the

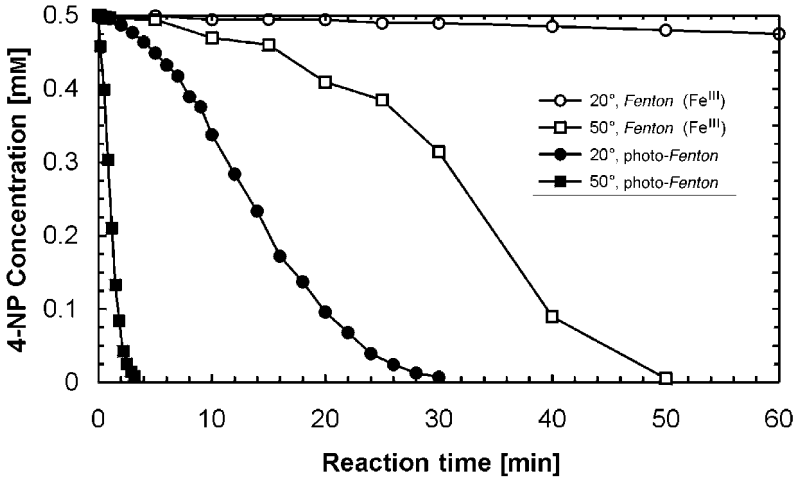

Fig. 9. *4-NP Concentration as a function of the reaction time at 20 and 50°.* Conditions as in *Fig. 6* or *7.*

photo-*Fenton* and the *Fenton* process, respectively. Within the limits of error of this data treatment, the apparent activation energies for both processes are, therefore, not distinguishable, and a mean value of $E_a = 47\ (\pm 7)$ kJ/mol results from this formal data treatment.

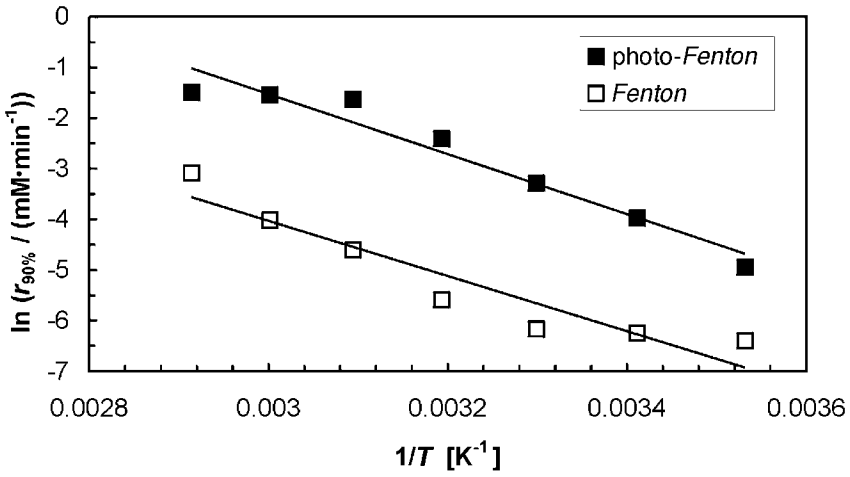

Fig. 10. *Logarithm of the reaction rate* $r_{90\%}$ *for the* Fenton *and the photo-*Fenton *process as a function of the reciprocal temperature*

Even though the exact mechanism for both processes is still under discussion, it can be postulated that the rate limiting steps are similar for the *Fenton* and photo-*Fenton* degradations of 4-NP. It is these rate-limiting reactions that are accelerated upon increasing temperature in both cases, resulting in formally indistinguishable apparent activation energies. It is well-known from respective studies of other AOPs, *i.e.*, photocatalysis, γ-radiolysis, and photolysis, that the degradation reactions involving

$OH^{\bullet}$ radicals and O_2 for the pollutant destruction exhibit only a rather small temperature dependence. Therefore, it is reasonable to assume that mainly the slowest reactions within the *Fenton* system itself, *e.g.*, reactions of *Eqns. 5–7* or even that of *Eqn. 2*, will be accelerated most significantly upon increasing the temperature within the reactor. However, the present study was not initiated to investigate mechanistic features in more detail. Moreover, it is not unrealistic to assume that different reaction rates will be accelerated with different temperature regimes and different systems (*Fenton* or photo-*Fenton*), respectively. Therefore, the apparent activation energies determined from *Fig. 10* cannot be correlated with a particular reaction but will be important for the layout of a pilot or full-scale plant for the ISFH process.

The photonic efficiency ξ is usually determined as the ratio of the observed rate of degradation to the rate of incident photons to compare different photochemical water-treatment processes. In analogy, we calculated a photonic efficiency for the degradation of 90% of the initially present substrate, $\xi_{90\%}$, using *Eqn. 20*, taking into account the rate of incident photons in the wavelength range 300–500 nm, where $q_{<500\,\mathrm{nm}}$ is the irradiance (in Einstein $\cdot\, m^{-2} \cdot s^{-1}$) within the wavelength range 300–500 nm, A_{inc} the irradiated reactor area, and V_{PR} the liquid volume of the photoreactor[1]).

$$\xi_{90\%} = \frac{\left(\frac{\Delta c}{\Delta t}\right)_{90\%} \cdot V_{\mathrm{PR}}}{q_{<500\,\mathrm{nm}} \cdot A_{\mathrm{inc}}} \tag{20}$$

Fig. 11 shows the photonic efficiency $\xi_{90\%}$, calculated from the results presented in *Fig. 7*, as a function of the reaction temperature. Following an almost exponential increase of $\xi_{90\%}$ with increasing temperature, it is obvious that, above 50°, the optimal conditions for the photo-*Fenton* process have been reached. Photonic efficiencies reaching 30% observed in the temperature range 50–70°, demonstrate that the photo-

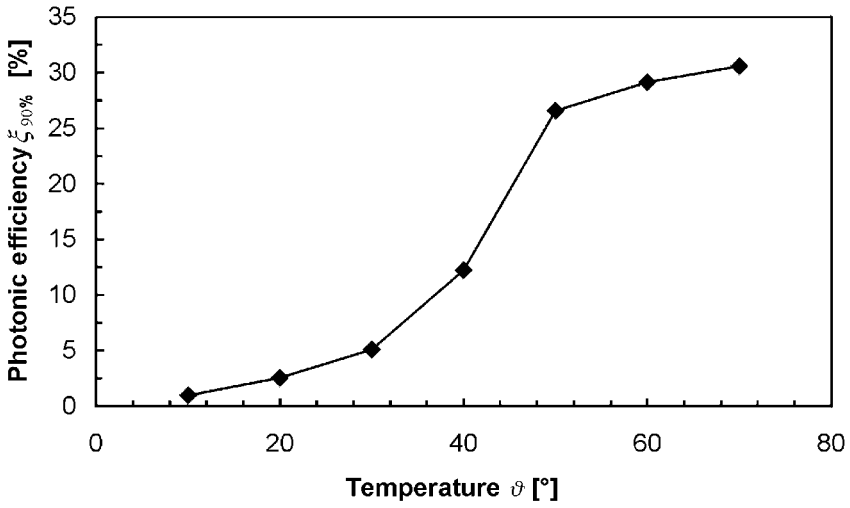

Fig. 11. *Photonic efficiency $\xi_{90\%}$ of the photo-*Fenton *process as a function of the temperature* (calculated from the results shown in *Fig. 7*)

Fenton process is clearly very attractive for the treatment of water polluted with molecules such as 4-NP when compared with alternative methods such as photocatalysis [20]. Moreover, due to its light-absorbing properties, the photo-*Fenton* process utilizes also photons within the VIS range, which is important, especially for solar applications of this technology.

It was already pointed out above that it is much more reasonable to compare photonic efficiencies than reaction rates, in particular, when experiments are performed under very different conditions. The photonic efficiencies $\xi_{90\%}$ were, therefore, also calculated for the data shown in *Fig. 8* and are presented in *Fig. 12* for 20 and 50°. It is obvious from these figures that $\xi_{90\%}$ increases continuously upon increasing the reactor depth for both reactor temperatures. This observation cannot simply be explained by an increased light absorption at greater reactor depth. As described earlier, a reactor depth of 1–2 cm will be sufficient to absorb nearly all incoming UV-A photons within the reactor. However, as the reactor depth is increased, more photons in the wavelength region 400–500 nm will be absorbed, which will result in an increased photochemical formation of Fe^{2+} from Fe^{3+} (*cf. Eqns. 14* and *15*) and, consequently, in a higher rate of the *Fenton* reaction (see *Eqn. 2*). These photochemical processes will result in a very homogeneous formation of Fe^{2+} throughout the entire reactor volume and hence to a very uniform distribution of $OH^{\bullet}$ radicals. Moreover, also Fe^{2+} formed *via* the absorption of UV-A photons in a very limited reactor volume at higher concentrations will be distributed rather homogeneously throughout the entire reactor volume, provided that the mixing is faster than the comparatively slow *Fenton* reaction. Overall, a larger reactor volume with homogeneously distributed reactants will favor the desired reactions over unwanted radical recombination processes or the oxidation of Fe^{2+} by free radical intermediates (see *Eqns. 12* and *13*).

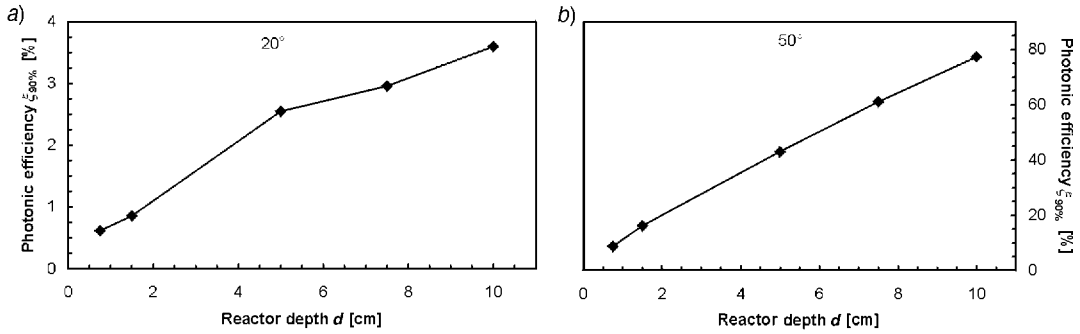

Fig. 12. *Photonic efficiency* $\xi_{90\%}$ *as a function of the reactor depth for the photo-*Fenton *process at* a) ϑ *20° and* b) ϑ *50°* (calculated from the results shown in *Fig. 8*)

It is obvious from the above discussion that the reactor depth represents an important parameter of the photo-*Fenton* process that needs to be optimized for the ISFH process. While an increased reactor depth results in an increased photonic efficiency, it has, however, serious disadvantages for the thermal behavior of the overall process. Since, for any solar application, the entire reactor volume has to reach the desired operating temperature every morning, there will be an upper limit for this total volume. We have used a rather simplistic energy balance to estimate the time to reach

elevated process temperatures for this non-steady-state heating problem. Neglecting any energetic requirements of the chemical reactions involved, the time-dependant energy change will be determined by the incoming energy flux $\dot{E}_{inc}$ and the energy flux to the surrounding environment $\dot{E}_{loss}$ (*Eqn. 21*).

With ρ_{H_2O} being the density of the effluent water, c_{H_2O} its heat capacity, q_{inc} the irradiance (in $W \cdot m^{-2}$), η_{abs} the efficiency to utilize the energy to heat the water, V_{PR} the reactor volume, and A_{inc} the irradiated area of the photoreactor[1]), *Eqn. 21* can be transformed to *Eqn. 22*. Assuming a flat-plate reactor with all incoming irradiation being utilized for the heating of the wastewater, *i.e.*, $\eta_{abs} = 1$, and neglecting energy losses, the upper limit of the temperature change $\Delta\vartheta$ can be calculated as a function of the irradiation time t by *Eqn. 23* at an illumination intensity of $1000\ W \cdot m^{-2}$.

$$\frac{\partial E}{\partial t} = \dot{E}_{inc} - \dot{E}_{loss} \tag{21}$$

$$\rho_{H_2O} V_{PR} c_{H_2O} \frac{\partial \theta}{\partial t} = \eta_{abs} q_{inc} A_{inc} - \dot{E}_{loss} \tag{22}$$

$$\Delta\vartheta = \frac{\eta_{abs} q_{inc} A_{inc}}{\rho_{H_2O} c_{H_2O} V_{PR}} t = \frac{\eta_{abs} q_{inc}}{\rho_{H_2O}\ c_{H_2O} d}\, t \tag{23}$$

Detailed models for flat-plate collectors that will be ultimately important for the construction of a pilot plant for the ISFH process are given in [26]. However, from *Eqn. 23* an upper limit for $\Delta\vartheta$ was calculated for various reactor depths as a function of the illumination time (see *Fig. 13*). Thus, even under these idealized conditions, it will take more than 30 min to heat the total water volume by 30°, *e.g.*, from 20 to 50°, if the reactor depth exceeds 1.5 cm. Since, under real solar conditions, the incoming illumination intensity is far below $1000\ W \cdot m^{-2}$, this heating time will be much longer. To reach the desired operation temperature of 50° within a reasonable process time, the reactor depth of a flat-plate reactor applicable to the ISFH process should, therefore, not exceed 1.5 to 2.0 cm. The optimal reactor depth will depend on various additional parameters such as actual climatic conditions, composition of the wastewater, and details of the process layout and should, therefore, be determined individually for each treatment plant.

Accelerated heating of the flat-plate reactor under solar conditions is only feasible if, *e.g.*, chemical energy from exothermal processes can be utilized which is the case for wastewater containing high TOC [13]. Additionally, storage of the hot wastewater overnight could reduce the time necessary to reach thermal steady-state conditions in the morning. Currently, the results presented here are utilized to design the first pilot facility for the realization of a continuous ISFH process.

Conclusions. – The ISFH process combines the photochemical utilization of solar energy for the photo-*Fenton* process with its thermal use. Thus, photons in the wavelength region 300 – 500 nm can induce the important photochemical conversion of Fe^{3+} to Fe^{2+}, while all photons ($\lambda > 300$ nm) can, in principle, provide thermal energy to increase the process temperature. Employing 4-nitrophenol (4-NP) as the model

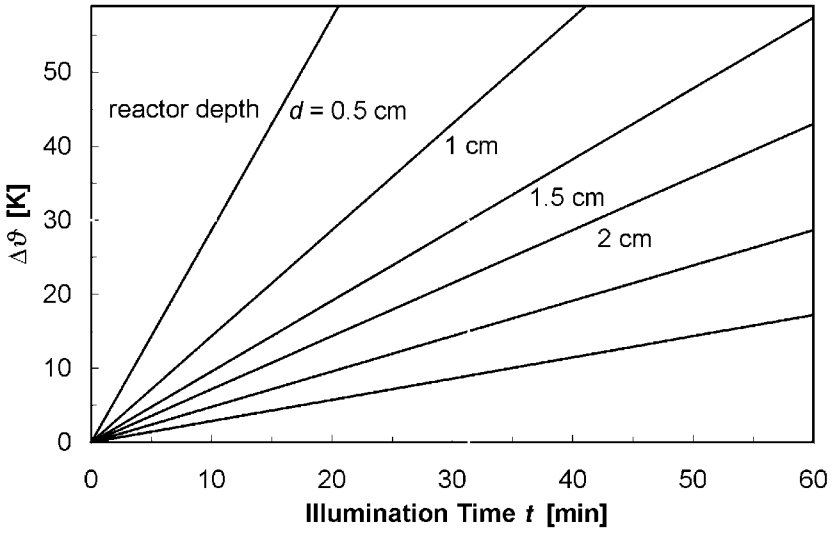

Fig. 13. *Temperature difference $\Delta\vartheta$ in a flat plate reactor as a function of the illumination time under idealized conditions for different reactor depths* d, *calculated with* Eqn. 23. $\eta_{abs} = 1.0$, $q_{inc} = 1000\ W \cdot m^{-2}$, $\dot{E}_{loss} = 0.0$, $c_{H_2O} = 4182\ J \cdot kg^{-1}$, $\rho_{H_2O} = 998\ kg \cdot m^{-3}$.

compound, we could show that, under the (nonoptimized) conditions used here, its rate of degradation increases by a factor of 125 when the reaction is carried out at 50° under simulated solar (AM 1.5) illumination rather than at 20° in the dark.

Data obtained from experiments at different temperatures exhibit a reasonable fit to an *Arrhenius*-type law with an apparent activation energy of $E_a = 47\ (\pm 7)$ kJ/mol being computed for both, the *Fenton* and the photo-*Fenton* process. Therefore, it is concluded that both reaction sequences are kinetically controlled by similar rate-limiting steps. Photonic efficiencies $\xi_{90\%}$, calculated for all photolytic degradation experiments, show that $\xi_{90\%}$ increases with increasing reactor depth, even far beyond the absorption limit in the UV-A region. While these results would suggest a reactor design with maximum depth, calculations regarding the time required for the reactor to reach a temperature 30° above ambient temperature suggest a maximum depth of 1.5–2.0 cm for a flat-plate reactor. The design of an optimized reactor for the continuous operation of the ISFH process, therefore, requires careful consideration of several important process parameters including the wastewater composition. Initial experiences with a first pilot plant for the ISFH process will be published soon.

Glossary

η_{abs}	efficiency to utilize irradiation
ϑ [°]	temperature in °
$\Delta\vartheta$ [K]	temperature difference
λ [nm]	wavelength
ρ_{H_2O} [$kg \cdot m^{-3}$]	density of water
$\xi_{90\%}$	photonic efficiency defined in *Eqn. 20*
4-NP	4-nitrophenol
A_{inc} [m^2]	irradiated area of a photoreacor

AM 1.5	air mass 1.5
AOPs	advanced oxidation processes
c [mmol · l^{-1}]	concentration
c_0 [mmol · l^{-1}]	initial concentration
$\Delta c_{90\%}$ [mmol · l^{-1}]	concentration difference for 90% degradation
c_{H_2O} [J · kg^{-1} · K^{-1}]	heat capacity of water
CPC	compound parabolic collector
d [m]	reactor depth (reactor bottom to solution surface)
DSSR	double-skin sheet reactor
E [J]	energy
E_a [kJ · mol^{-1}]	apparent *Arrhenius* activation energy
$\dot{E}_{loss}$ [W]	rate of energy loss
$\dot{E}_{inc}$ [W]	rate of incident energy
ISFH	insulated solar *Fenton* hybrid
LMCT	ligand-to-metal charge transfer
PMMA	poly(methyl methacrylate)
PTR	parabolic trough reactor
$q_{<500\,nm}$ [Einstein · m^{-2} s^{-1}]	irradiance ($\Delta\lambda = 300-500$ nm)
q_{UV} [W · m^{-2}]	UV irradiance ($\Delta\lambda = 300-400$ nm)
q_λ [W · m^{-2} · nm^{-1}]	spectral irradiance (at the top of the photoreactor)
q_{ref} [W · m^{-2} · nm^{-1}]	reference spectral irradiance
$q_{\lambda rel}$	relativ spectral irradiance (defined by *Eqn. 17*)
$r_{90\%}$ [mmol · l^{-1} min^{-1}]	reaction rate defined in *Eqn. 19*
T [K]	temperature in K
t [s]	time
$\Delta t_{90\%}$ [s]	time to reach 90% degradation
TOC [ppm]	total organic carbon
V_{PR} [m^3]	liquid volume of photoreactor

REFERENCES

[1] J. H. Carey, *Water Poll. Res. J. Canada* **1992**, *27*, 1.
[2] R. Bauer, H. Fallmann, *Res. Chem. Intermed*. **1997**, *23*, 341.
[3] R. Chen, J. J. Pignatello, *Environ. Sci. Technol*. **1997**, *31*, 2399.
[4] J. J. Pignatello, *Environ. Sci. Technol*. **1992**, *26*, 944.
[5] R. G. Zepp, B. C. Faust, J. Hoigné, *Environ. Sci. Technol*. **1992**, *26*, 313.
[6] Y. Sun, J. J. Pignatello, *Environ. Sci. Technol*. **1993**, *27*, 304.
[7] E. Lipczynska-Kochany, *Water Poll. Res. J. Canada* **1992**, *27*, 97.
[8] A. Safarzadeh-Amiri, J. R. Bolton, S. R. Cater, *J. Adv. Oxid. Technol*. **1996**, *1*, 18.
[9] E. Oliveros, O. Legrini, M. Hohl, T. Müller, A. M. Braun, *Water Sci. Technol.* **1997**, *35*, 223.
[10] H. Fallmann, T. Krutzler, R. Bauer, S. Malato, J. Blanco, *Catal. Today* **1999**, *54*, 309.
[11] T. Krutzler, H. Fallmann, P. Maletzky, R. Bauer, S. Malato, J. Blanco, *Catal. Today* **1999**, *54*, 321.
[12] E. Balanosky, F. Herrera, A. Lopez, J. Kiwi, *Water Res.* **2000**, *34*, 582.
[13] T. Renner, A. Reichelt, I. Wurdack, O. Specht, D. Wabner, 'Second International Conference on Oxidation Technologies for Water and Wastewater Treatment', CUTEC-Schriftenreihe Nr. 46, Ed. A. Vogelpohl, Papierflieger Verlag, Clausthal-Zellerfeld, 2000, p. 39.
[14] G. Sagawe, M. Lübber, G. Rockendorf, D. Bahnemann, '12. Internationales Sonnenforum: Sonne – Die Energie des 21. Jahrhunderts', Freiburg, July 05 – 07, 2000, Tagungsband, p. 619.
[15] H. J. H. Fenton, *Chem. Soc*. **1894**, *65*, 899.
[16] C. Walling, *Acc. Chem. Res.* **1975**, *8*, 125.
[17] J. J. Pignatello, D. Liu, P. Huston, *Environ. Sci. Technol*. **1999**, *33*, 1832.
[18] S. H. Bossmann, E. Oliveros, S. Göb, S. Siegwart, E. P. Dahlen, L. Payawan Jr., M. Staub, M. Wörner, A. M. Braun, *J. Phys. Chem*. **1998**, *102*, 5512.
[19] K. Ito, J. Hu, M. Yang, *Environ. Technol.* **1998**, *19*, 183.

[20] D. Bahnemann, in 'The Handbook of Environmental Chemistry', Vol. 2, Reactions and Processes, Part L, Environmental Photochemistry, Ed. P. Boule, Series Ed. O. Hutzinger, Springer Verlag, Heidelberg, 1999, p. 285.
[21] D. Bahnemann, R. Dillert, J. Dzengel, R. Goslich, G. Sagawe, H.-W. Schumacher, V. Benz, *J. Adv. Oxid. Technol*. **1999**, *4*, 11.
[22] F. Herrera, C. Pulgarin, V. Nadtochenko, J. Kiwi, *Appl. Catal., B* **1998**, *17*, 141.
[23] O. M. Alfano, D. Bahnemann, A. E. Cassano, R. Dillert, R. Goslich, *Catal. Today* **2000**, *58*, 199.
[24] R. E. Bird, R. L. Hulstrom, L. J. Lewis, *Solar Energy* **1983**, *30.*, 563.
[25] Dr. K. Hönle GmbH, 'UV-Technologie' (product information), Martinsried, 2001.
[26] J. A. Duffie, W. A. Beckman, 'Solar Engineering of Thermal Processes', 2nd edn., Wiley-Interscience, New York, 1991.

Received June 14, 2001